Effect of inter-filament distance on the improvement of Reverse Osmosis desalination process

M. AMOKRANE[a,b], D. SADAOUI[a], M. DUDECK[b]

[a] Laboratoire de Mécanique, Matériaux et Energétique (L2ME), Faculté de Technologie, Université de Bejaia, 06000 Bejaia, Algérie. mounir139@live.fr (M. AMOKRANE), sadaouidjamel@yahoo.fr (D. SADAOUI)
[b] Institut d'Alembert, UMR 9071, CNRS et Université Pierre et Marie Curie, 4 place Jussieu, 75252 Paris, France. michel.dudeck@upmc.fr

Résumé:

Dans la littérature, plusieurs papiers ont été consacrés à l'étude numérique du champ hydrodynamique et du champ de concentration à l'intérieur des modules membranaires, ou le degré de complexité de modèles développés variée d'un article à un autre. Ce papier présente un modèle CFD bidimensionnel qui prend en considération la polarisation de concentration qui se développe le long des membranes, le flux de perméation et la variation locale des paramètres physiques des solutions salines. Ce modèle numérique est utilisé pour analyser les performances des différentes configurations (zigzag, immergée et cavité) en variant la distance entre deux obstacles successifs. Les évolutions locales et moyennes le long des membranes comme le dépôt de sel, le flux de perméation et le nombre de Sherwood sont examinés pour divers vitesses de circulation. Les résultats numériques montrent que pour les configurations zigzag et immergée, le rendement est meilleur (moins de dépôt de soluté, flux de perméation et nombre Sherwood élevés) lorsque le ratio l/H = 2. Tandis que pour la configuration cavité, le flux de perméation et le dépôt de soluté sont meilleurs lorsque l/H = 3.

Abstract:

Various numerical studies that exhibit flow field and mass transfer inside membrane channels can be found in the literature; however the complexity and the accuracy differs from one to another. This paper deal with the study of two-dimensional CFD model taking account both the permeation flux; concentration polarization along membrane surfaces and variable physical properties. The model analyzes the effect of the inter-filaments length in three different configurations (zigzag, cavity and submerged). Local evolution and averaged values of mass deposit, permeation flux and Sherwood number were examined for three different inlet velocities. Numerical results showed that in zigzag and submerged configurations, the highest efficiency (low concentration polarization, high permeation flux and Sherwood number) is achieved with a geometric ratio l/H = 2. While in cavity configuration, mass deposit and enhancement of the permeation flux can be higher with an aspect ratio l/H = 3.

Key words: Concentration polarization, CFD, desalination, Reverse osmosis, Spiral wound membrane module.

1 Introduction

Nowadays, Reverse Osmosis is the widely used process for the desalination of sea and brackish waters, because most plants use this technology which is more economical and more attractive than other process of desalination. The essential part of RO plants is membrane modules that work as selective barriers for the retention of solutes. Since eighties, many researchers studied experimentally flows and the physical phenomena that occur within these modules [1]. However, in the recent years with the development of numerical tools, many numerical studies emerged as mentioned in the recent review [2]. One of phenomena that cause the reduction of the efficiency of an RO filtration is named 'concentration polarization'. This polarized boundary layer that develops on membrane walls due to the convection-diffusion is irreversible, thus many numerical studies were aimed to model them, especially within plan channels [3-8].

In order to reduce the concentration polarization and enhance the process; current spiral wound membrane modules (SWM) contain spacers arranged in different configurations as zigzag, submerged and cavity such that, many CFD studies were conducted within these geometries. Cao et al [9] modeled turbulent flows for submerged and zigzag configurations using a commercial code. Results showed that the presence of spacers increases the shear stress near membrane walls, also they suggested that submerged configuration is more efficient. Shwinge et al [10-13] conducted various numerical studies in order to optimize commercial membrane channels. They varied geometrical parameters and exhibited the flow field within different configurations [10], then they studied transition areas depending of the spacer configuration [11]. In another paper, they followed evolution of recirculation zones that form behind spacers for each configuration [12]. Finally, mass transfer was studied in depth for the same configurations function of geometrical parameters and inlet velocity [13]. Geraldes et al [14-16] focused on the study of flows and concentration fields within ladder type spacers (square) using a quasi-periodic boundary condition. First, they considered only hydrodynamic field by varying geometrical parameters [14]; thereafter, mass transfer was introduced in the model and concentration polarization was estimated [15-16]. Using the same boundary condition, Koutsou et al [17] simulated an array of submerged spacers to better understand transient flows. Many parameters were examined as shear stress, pressure drop and other statistical parameters. Later, Ma et al [18-19] developed a numerical model using Petrov/Galerking method to resolve hydrodynamic and mass transfer equations within channels containing square spacers. They focused on the effect of varying geometrical parameters on mass transfer. Subramni et al [20] studied mass transfer within an open channels and spacer channels representing submerged, zigzag and cavity configurations. They showed that the use of spacers reduces drastically concentration polarization, but for zigzag configurations, the probability of fouling is relatively high. Soon thereafter, Wardeh and Morvan [21] simulated channels filled by various spacers in different configurations. Permeability, solute accumulation, pressure drop and shear stress were predicted and compared. Results highlighted that zigzag configuration achieves the best performance but may promote the fouling. More recently, Amokrane et al [22] developed a time-dependent model to study the flow filed and concentration polarization for spacer filled channels. Two configurations were studied and key parameters exhibited in term of spatial and temporal values. Furthermore, it's suggested that zigzag disposition is more desirable to enhance the desalination. It's noteworthy to note that we can distinguish in the literature several studies regarding the optimization process by designing new spacer shapes [23-26].

Previously, Amokrane el al [22] presented a detailed investigation of fluid flow and concentration polarization for various spacer configurations. The study was conducted within long channels filled by various spacers, which consumed much computation resources. Also, geometric parameters were fixed constant. The aim of this paper is to use a complete two-dimensional model encompassing all essential phenomena occurring within a spiral wound membrane module to predict locally and averagely, concentration polarization, water permeability and other key parameters for various geometrical ratios (inter-filaments length / channel height) in zigzag, cavity and submerged configurations.

2 Modeling

Geometries of interest are shown in Fig. 1. It shows a two-dimensional cross section (unit cell) of a spiral wound membrane module arranged in various configurations: (a) zigzag, (b) cavity and (c) submerged. In all simulations, the height of channels (H) and the diameter of spacers (d) are maintained constant; only the distance between the filaments (*l*) and channel lengths (L) vary. In this regards, the ratio H/d = 2, while *l* = 4, 6 and 8 corresponding to channel lengths L = 8, 12 and 16, respectively. The diameter d of the spacers is the same in all configurations.

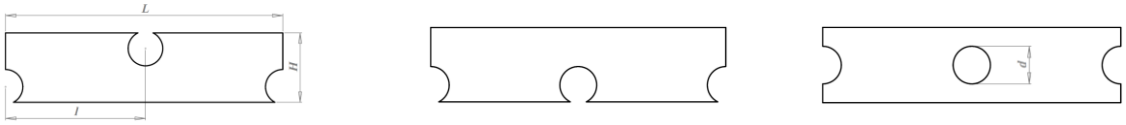

(a) (b) (c)

Figure.1. Geometries of interest: (a) zigzag, (b) cavity and (c) submerged

In the current study, some assumptions were taken to model numerically the fluid flow and the mass transfer. In fact, the flow is assumed isothermal, laminar and incompressible; while effects of gravity, viscous dissipation and compressibility are neglected. Under these assumptions, the equations of continuity, momentum and mass transfer are cast in their dimensionless form as follow:

$$\left.\begin{aligned} &\frac{\partial \rho}{\partial t} + \nabla.\left(\rho \boldsymbol{V}\right) = 0 \\ &\frac{\partial \rho \boldsymbol{V}}{\partial t} + \nabla.\left(\rho \boldsymbol{V}\boldsymbol{V}\right) = \nabla.\left[\mu\left(\nabla \boldsymbol{V} + \nabla \boldsymbol{V}^{T}\right)\right] - \nabla p \\ &\frac{\partial \rho m_A}{\partial t} + \nabla.\left(\rho \boldsymbol{V} m_A\right) = \nabla \cdot \left(\rho D_{AB} \nabla m_A\right) \end{aligned}\right\} \qquad (1)$$

In above equations ρ, μ, **V** and p are the density, dynamic viscosity, velocity field and pressure while m_A and D_{AB} are the salt mass fraction and the binary diffusion coefficient of the solute A in the solvent B, respectively.

Physical properties of the aqueous solution of sodium chloride (NaCl) vary according to Eqs. (2)- (5) as described by Geraldes et al [3] and valid for a mass fraction not exceeding 0.09 kg/kg.

$$\pi = 805.1 \times 10^5 \, m_A \qquad (2)$$

$$\mu = 0.89 \times 10^{-3}(1+1.63m_A) \quad (3)$$

$$D_{AB} = \max(1.61 \times 10^{-9}(1-14m_A), 1.45 \times 10^{-9}) \quad (4)$$

$$\rho = 997.1 \times (1.0 + 0.696m_A) \quad (5)$$

Following boundary conditions are applied at the different boundaries of the simulated domain:

At channel inlets (x = 0; 0 ≤ y ≤ H)

$$m_{A0} = 0.002 \qquad v = 0 \qquad u = u_o \quad (6)$$

At channel outlets (x = L; 0 ≤ y ≤ H)

$$\frac{\partial u}{\partial x} = 0 \qquad \frac{\partial v}{\partial x} = 0 \qquad \frac{\partial m_A}{\partial x} = 0 \quad (7)$$

On spacers

$$u = 0 \qquad v = 0 \qquad \frac{\partial m_A}{\partial x} = 0 \quad (8)$$

Membrane walls (y = 0, y = H) are assumed impermeable (perfect semi-permeable membranes) to the salt and having a constant salt rejection (R = 99%) and membrane resistance (R_m = 1562 x 10^{14} m^{-1}) [22, 26]. A constant trans-membrane pressure is taken for all simulations (ΔP = 8.103 10^5 Pa), then no simulation of the water flow is required out of the membranes.

A coupled boundary condition which links concentration polarization and permeation flux is applied on membranes surfaces (y = 0; y = H ; 0 ≤ x ≤ L)

$$\left.\begin{aligned} u &= 0 \\ v &= \pm J_v = \pm \frac{1}{R_m \mu_w}\left(\Delta P - \Delta\pi\right) \\ J_v . R . m_A &= -D_{AB}\frac{\partial m_A}{\partial y} \end{aligned}\right\} \quad (9)$$

The positive sign (+) indicates the upper membrane surface, while the negative (-) represent the lower membrane surface. In previous equation, μ_w is the dynamic viscosity of the pure water and J_v the permeate flux; which vary along membranes walls according to the trans-membrane pressure ΔP and osmotic pressure Δπ.

Concentration polarization due to the accumulation of the rejected solutes on the membrane walls promotes the formation of a polarized layer thickness along membranes surfaces. From film theory this layer thickness is calculated using Eq. (12), [6].

$$\delta = \ln\left(\frac{m_{Am}\,R}{m_{A0}-(1-R)m_{Am}}\right)\times\frac{D_{AB}}{J_v} \tag{10}$$

Therefore, Sherwood number for un-fouled membrane is calculated using Eq. (11):

$$Sh = \frac{k.d}{D_{AB}} \tag{11}$$

where k , is the mass transfer coefficient related to concentration layer thickness by the following formulation $k = (D_{AB}/\delta)$.

3 Numerical procedure

Governing equations of the continuity, momentum and mass transfer (Eq. 1) with the prescribed boundary conditions are solved numerically by the finite volume method under non-uniform grid system in x and y directions. The developed solver uses a pressure correction based on iterative SIMPLE algorithm. Convective terms were discretized using the second order upwind scheme; however for some cases (submerged configuration, $u_0 \geq 0.15$ m/s) time-dependent approximation was adopted and the second order Adams-Moulton scheme applied for the time discretization. To check the convergence of the sequential iterative solution, the normalized residual was calculated for the mass, momentum and mass transfer equations. Thus the convergence is obtained when the residual factor becomes smaller than 10^{-8}. To achieve a solution independent of the mesh, computational grids sizes were varied between 11100 and 11890 nodes depending on the chosen configuration. Moreover, the mesh was refined and focused near membrane walls and spacers, where the largest gradients of velocity and mass fraction are located.

3.1 Validation of the model

Furthermore, extensive validations of the developed code for the concentration polarization along the membrane wall have been also validated against the results reported by Pinho et al [4] and Ahmad et al [5], in an open channel (without spacers). The computations have been performed in term of concentration polarization factor ($\Gamma = (m_A - m_{A0})/ m_{A0}$) for various trans-membranaire pressure (1; 2 and 3). As shown in figure 2, our prediction seems to be in agreement with these of references [4] and [5].

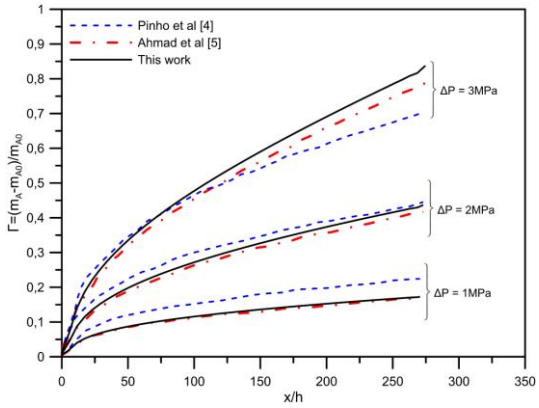

Figure 2. Comparison of concentration polarization factor between current work and references [4] and [5]

4 Results and discussion

In this study, the inlet velocity (u_0) varies between 0.1 and 0.2 m/s which is sufficient to ensure flow velocities in real application [17]. In addition, to avoid any entrance effect, established profiles were applied at channel entrances.

The flow structure is visualized for the different configurations and various geometric ratios (l/H). Thus, Fig. 3 shows contours of velocity magnitude within different channels for the aspect ratio l/H = 2 and 4. For zigzag and cavity configurations, the flow remains stable, while in submerged configuration, instabilities appear; which is in accordance with the literature findings (refs [10, 17, and 22]). Further, increasing the length between two successive filaments reduces the region of high velocity gradients (red contours) and the main flow is separated between the two spacers. Meanwhile, the submerged configuration seems less affected by the inter-filaments length.

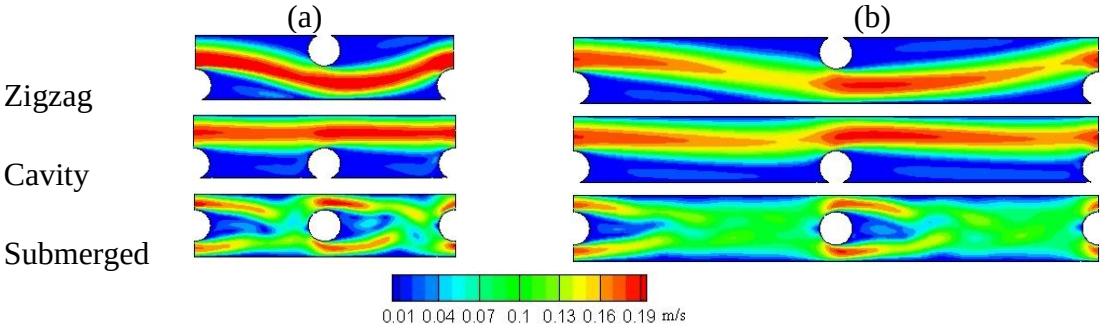

Figure 3. Contours of velocity magnitude for various configurations ($u_0 \approx 0.198$ m/s)
(a) $l/H = 2$; (b) $l/H = 4$

To better analyze the effect the inter-filaments distance (l) on both the concentration field and the development of concentration polarization, numerical simulations are performed for three ratios (l/H = 2, 3, and 4) and three input flow velocities ($u_0 \approx 0.1$, 0.15, and 0.2 m/s). Corresponding results are presented in term of local and averaged values.

Fig. 4 depicts contours of mass fraction for the different configurations at various geometrical ratios (l/H). For the submerged configuration, increasing the distance between two successive spacers generates more disturbances in concentration boundary layer near membrane walls. In the zigzag and cavity configurations, the increasing of the geometric ratio allows the increase of the water salinity, particularly within the recirculation zones localized upstream and downstream the spacers. Nevertheless, the concentration still constant inside the main flow, and the normal gradient mass concentration near the membranes decreases between two spacers with the increase of l.

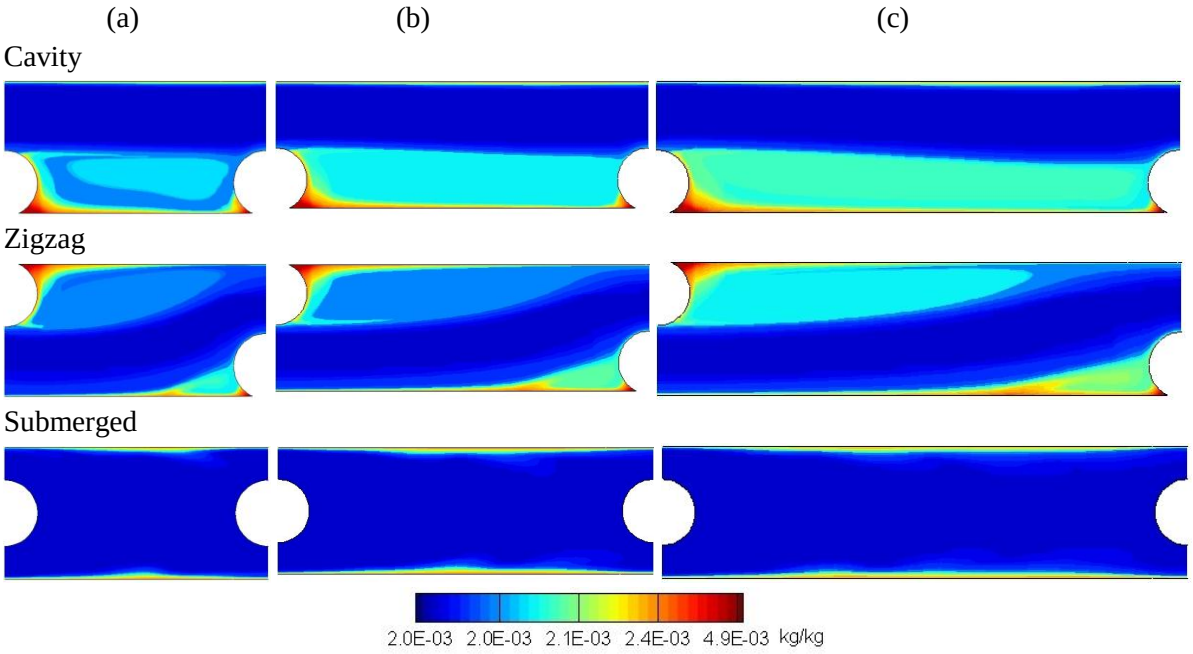

Figure 4. Contours of mass fraction at various aspect ratios: (a) *l*/H=2, (b) *l*/H=3 and (c) *l*/H=4; $u_0 \approx$ 0.19 m/s

Profiles of the local concentration polarization are exhibited in Fig. 5 for the three studied configurations. Increasing the length between two successive filaments expands the development of concentration polarization and moves the separation point (S). Furthermore, the local value of the concentration in the vicinity of the attachment point (spacer - membrane) increases. For cavity configuration, local evolutions are relatively similar depending on the length, only values vary. However, in submerged configuration, local profiles differ; this is due to the vortices that develop between the obstacles. It is noted that vortices are numerous and stronger when obstacles are widely spaced.

Local variations of Sherwood number along the lower membrane surface are shown in Fig. 5b. For the zigzag configuration, the maximum values is obtained for a geometrical ratio *l*/H=2; the increase of this ratio causes a reduction in local values. The same trend is noticed for cavity and submerged configurations, the increasing of the inter filament length causes a stretching of local profiles which reduce local values

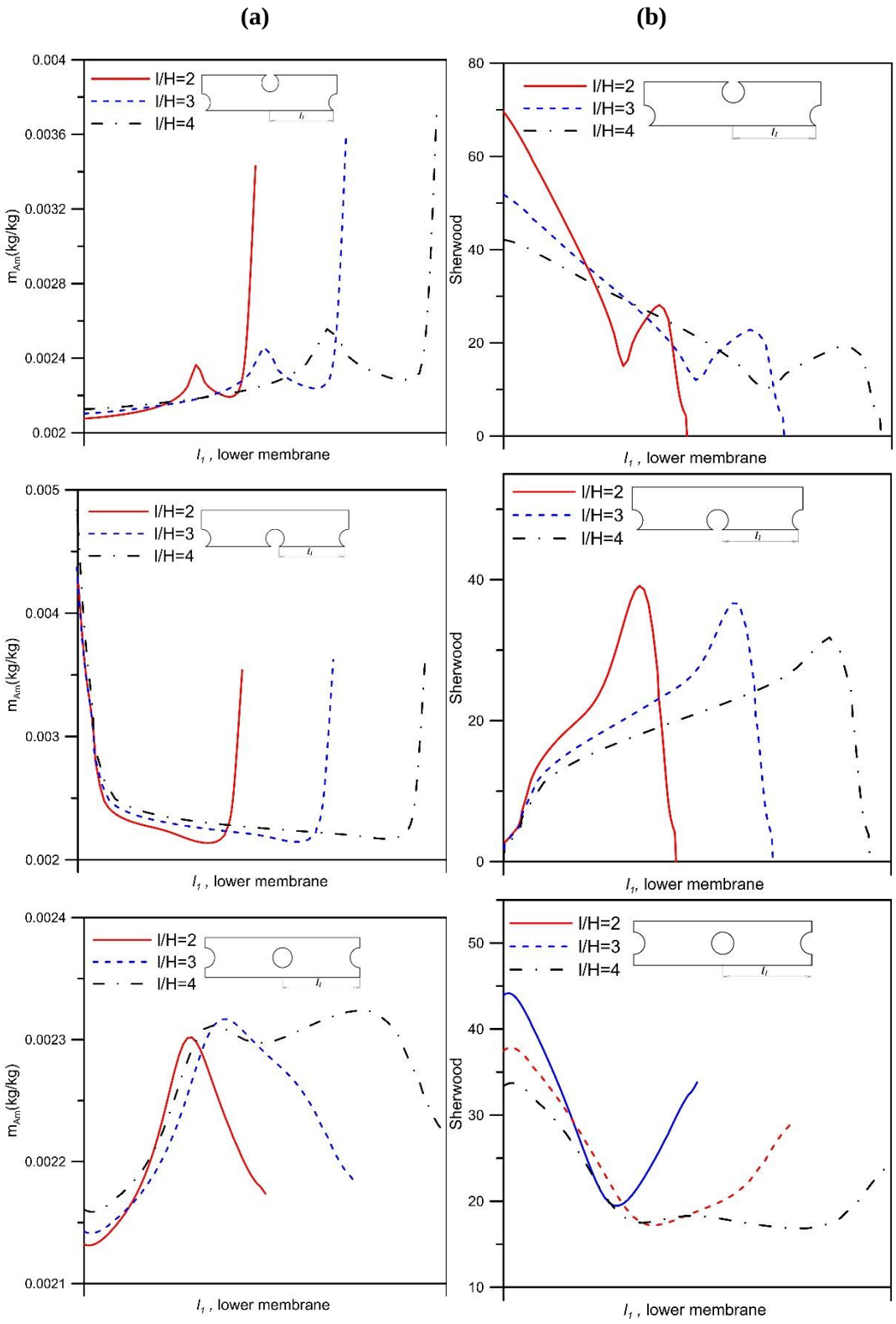

Figure. 5 Local distributions of concentration polarization (a) and Sherwood number (b) along the length l_1 for various configurations and various geometrical ratios; $u_0 \approx 0.19$ m/s

In order to compare efficiency of various spacer configurations, averaged values of key parameters (i.e. m_{Am}, J_v and Sh) along the lower membrane surface are summarized in table 1. It is worthy to note that whatever the chosen configuration, the increase of inlet velocity reduces the concentration of polarization and improves the permeation flux and the Sherwood number [22]. Concerning the effect of the geometric ratio (*l*/H), the same trend is observed for zigzag and submerged configurations, where the minimum of (ma) and the maximum of (Jv) are obtained when the ratio *l*/H=2. An increase of this ratio causes a decrease of the performances.

In cavity configuration, for low velocity (0.1 m/s), the ratio *l*/H = 4 causes best performance in term of cleaning membranes and producing pure water. For higher velocities (0.15 to 0.2) spacer channels with an aspect ratio *l*/H=3 admit the best compromise between reducing concentration polarization and permeation flux. However, it should be noted that the highest Sherwood number is obtained with a ratio *l*/H= 2.

(a) Zigzag

	l/H = **2**			*l*/H = 3			*l*/H = 4		
u_0 m/s	$\bar{m}_{Am}$ kg/kg	$\bar{J}_v.10^{-6}$ m/s	$\bar{Sh}$	$\bar{m}_{Am}$ kg/kg	$\bar{J}_v.10^{-6}$ m/s	$\bar{Sh}$	$\bar{m}_{Am}$ kg/kg	$\bar{J}_v.10^{-6}$ m/s	$\bar{Sh}$
0.1	0.002321	3.973	27.31	0.002356	3.957	22.01	0.002383	3.945	18.97
0.15	0.002265	4.000	34.26	0.002288	3.992	27.77	0.002316	3.980	23.57
0.2	0.002237	4.014	40.06	0.002252	4.011	32.79	0.002275	4.001	27.84

(b) Cavity

	l/H = 2			*l*/H = 3			*l*/H = 4		
u_0 m/s	$\bar{m}_{Am}$ kg/kg	$\bar{J}_v.10^{-6}$ m/s	$\bar{Sh}$	$\bar{m}_{Am}$ kg/kg	$\bar{J}_v.10^{-6}$ m/s	$\bar{Sh}$	$\bar{m}_{Am}$ kg/kg	$\bar{J}_v.10^{-6}$ m/s	$\bar{Sh}$
0.1	0.002513	3.862	16.22	0.002492	3.880	14.32	0.002467	3.897	15.20
0.15	0.002464	3.887	18.92	0.002421	3.917	18.22	0.002444	3.909	15.55
0.2	0.002434	3.902	21.06	0.002392	3.934	20.58	0.002395	3.931	18.94

(c) Submerged

	l/H = 2			*l*/H = 3			*l*/H = 4		
u_0 m/s	$\bar{m}_{Am}$ kg/kg	$\bar{J}_v.10^{-6}$ m/s	$\bar{Sh}$	$\bar{m}_{Am}$ kg/kg	$\bar{J}_v.10^{-6}$ m/s	$\bar{Sh}$	$\bar{m}_{Am}$ kg/kg	$\bar{J}_v.10^{-6}$ m/s	$\bar{Sh}$
0.1	0.002195	4.047	25.38	0.002251	4.008	19.61	0.002289	3.991	16.8
0.15	0.002181	4.054	28.93	0.002222	4.023	22.58	0.002243	4.015	20.48
0.2	0.002164	4.063	30.45	0.002206	4.031	25.19	0.002235	4.019	21.39

Table 1. Averaged values of mass deposit, permeation flux and Sherwood number for various aspect ratios *l*/H and inlet velocities: (a) cavity; (b) zigzag and (c) submerged configurations

5 Conclusion

A complete two dimensional CFD model was used to study the effect of varying the inter-filament length on the development of concentration polarization, permeation flux and Sherwood number inside 'unit cell' representing three different spacer channels.

Numerical predictions showed that for zigzag and submerged configurations, the process admits the best performances with an aspect ratio (*l*/H=2). In general, increasing the distance between two successive spacers promotes salt deposition on membrane surfaces which reduces both permeation flux and transfer efficiency (Sh).

The study suggests the reduction of the inter-filaments length as a way to control the development of concentration polarization and thus reduce the probability of fouling.

Nomenclature

d	diameter of the spacers (m)
D_{AB}	binary diffusion coefficient (m^2/s)
H	channel height (m)
J_v	permeation flux (m/s)
k	mass transfer coefficient (m/s)
L	total channel length (m)
l	inter-filament length (m)
m_A	salt mass fraction (kg solution/ kg solution)
P	pressure (Pa)
R	intrinsic rejection coefficient ($1-(m_{Ap}/m_{Am})$)
R_m	hydraulic resistance of the membrane (m^{-1})
Sh	Sherwood number ($Sh = k.d / D_{AB}$)
V	fluid velocity field (m/s)
u, v	velocity components in Cartesian coordinates (m/s)
x, y	Cartesian coordinates (m)

Greek letters

δ	concentration polarization layer thickness (m)
ρ	density (kg/m^3)
μ	dynamic viscosity (Pa.s)
ΔP	trans-membranaire pressure (Pa)
$\Delta\pi$	osmotic pressure (Pa)

Subscripts

0	inlet channel
m	membrane surface
w	pure water

References

[1] G. Shock, A. Miquel, Mass transfer and pressure loss in spiral wound modules, Desalination 64(1987)339–352.

[2] A.J. Karabelas, M. Kostoglou, C.P. Koutsou, Modeling of spiral wound membrane desalination modules and plants – review and research priorities, Desalination, 356 (2015) 165-186.

[3] V. Geraldes, V. Semião, M.M. Pinho, Flow and mass transfer modelling of nanofiltration, J. Membr. Sci., 191 (2001) 109–128.

[4] M. N. Pinho, V. Semião, V. Geraldes, Integrated modeling of transport processes in fluid/nanofiltration membrane systems, J. Membr. Sci., 206 (2002) 189–200.

[5] A .L. Ahmad, K.K. Lau, M.Z. Abu Bakar, S.R. Abd. Shukor, Integrated CFD simulation of concentration polarization in narrow membrane channel, Comput. Chem. Eng., 29 (2005) 2087-2095.

[6] D. E .Wiley, D .F. Fletcher, Techniques for computational fluid dynamics modeling of flow in membrane channels, J. Membr. Sci., 211 **(**2003) 127–137.

[7] D.F. Fletcher, D.E. Wiley, A computational fluids dynamics study of buoyancy effects in reverse osmosis, J. Membr. Sci., 245 (2004) 175–181.

[8] M. Kostoglou, A. J. Karabelas, Comprehensive simulation of flat-sheet membrane element performance in steady state desalination, Desalination, 316 (2013) 91–102.

[9] Z. Cao, D.E. Wiley, A.G. Fane, CFD simulations of net-type turbulence promoters in a narrow channel, J. Membr. Sci., 185 (2001) 157–176.

[10] J. Schwinge, D. E. Wiley, D. F. Fletcher, Simulation of the Flow around Spacer Filaments between Narrow Channel Walls. 1. Hydrodynamics, Ind. Eng. Chem. Res., 41 (2002) 2977-2987.

[11] J. Schwinge, D. E. Wiley, D. F. Fletcher, Simulation of the Flow around Spacer Filaments between Channel Walls. 2. Mass-Transfer Enhancement, Ind. Eng. Chem. Res., 41 (2002) 4879-4888.

[12] J. Schwinge, D.E. Wiley, D.F. Fletcher, A CFD study of unsteady flow in narrow spacer-filled channels for spiral wound membrane modules, Desalination, 146 (2002) 195–201.

[13] J. Schwinge, D.E. Wiley, D.F. Fletcher, Simulation of unsteady flow and vortex shedding for narrow spacer-filled channels, Ind. Eng. Chem. Res.,42 (2003) 4962–4977.

[14] V.Geraldes, V.Semião, M.N. Pinho, Flow management in nanofiltration spiral wound modules with ladder-type spacers, J. Membr. Sci., 203 (2002) 87–102.

[15] V. Geraldes , V. Semião , M .N. Pinho, The effect of the ladder-type spacers configuration in NF spiral-wound modules on the concentration boundary layers disruption, Desalination, 146 (2002) 187–194.

[16] V. Geraldes, V. Semião, M. N. Pinho, Hydrodynamics and Concentration polarisation and flow structure within nanofiltration spiral-wound modules with ladder-type spacers, Desalination, 157 (2003) 395-402.

[17] C.P. Koutsou, S.G. Yiantsios, A.J. Karabelas, Numerical simulation of the flow in a plane-channel containing a periodic array of cylindrical turbulence promoters, J. Membr. Sci., 231 (2004) 81–90.

[18] S. Ma, L. Song, S.L. Ong, W. J. Ng, A 2-D streamline upwind Petrov/Galerkin finite element model for concentration polarization in spiral wound reverse osmosis modules, J. Membr. Sci., 244 (2004) 129–139.

[19] S. Ma, L. Song, Numerical study on permeate flux enhancement by spacers in a crossflow reverse osmosis channel, J. Membr. Sci., 284 (2006) 102–109.

[20] A. Subramani, S. Kim, E. M.V. Hoek, Pressure, flow, and concentration profiles in open and spacer-filled membrane channels, J. Membr. Sci., 277 (2006) 7–17.

[21] S. Wardeh, H.P. Morvan, CFD simulations of flow and concentration polarization in spacer-filled channels for application to water desalination, Chem. Eng. Res. Des., 86 (2008) 1107–1116.

[22] M. Amokrane, D. Sadaoui, C.P. Koutsou, A.J. Karabelas, M. Dudeck, A study of flow field and concentration polarization evolution in membrane channels with two-dimensional spacers during water desalination, J. Membr. Sci. 477 (2015) 139–150.

[23] A .L. Ahmad, K.K. Lau, Impact of different spacer filaments geometries on 2D unsteady hydrodynamics and concentration polarization in spiral wound membrane channel, J. Membr. Sci., 262 (2005) 138–152.

[24] A.L. Ahmad, K.K. Lau, M.Z. Abu Bakar, Impact of different spacer filament geometries on concentration polarization control in narrow membrane channel, J. Membr. Sci., 286 (2006) 77–92.

[25] G. Guillen, E. M.V. Hoek, Modeling the impacts of feed spacer geometry on reverse osmosis and nanofiltration processes, Chem. Eng. J., 149 (2009) 221–231.

[26] M. Amokrane, D. Sadaoui, M. Dudeck, C.P. Koutsou (2015): New spacer designs for the performance improvement of the zigzag spacer configuration in spiral-wound membrane modules, Desalination and Water Treatment, DOI: 10.1080/19443994.2015.1022003